CELL BIOLOGY

# Extracellular fluid viscosity regulates human mesenchymal stem cell lineage and function

**Alice Amitrano[1,2]†, Qinling Yuan[1,2]†, Bhawana Agarwal[1,2]‡, Anindya Sen[1,2]‡, Yoseph W. Dance[2,3]‡, Yi Zuo[2,4]‡, Jude M. Phillip[1,2,3,5], Luo Gu[2,4], Konstantinos Konstantopoulos[1,2,3,5]***



**Human mesenchymal stem cells (hMSCs) respond to mechanical stimuli, including stiffness and viscoelasticity. To date, it is unknown how extracellular fluid viscosity affects hMSC function on substrates of different stiffness and viscoelasticity. While hMSCs assume an adipogenic phenotype on gels of low stiffness and prescribed stress relaxation times, elevated fluid viscosity is sufficient to bias hMSCs toward an osteogenic phenotype. Elevated viscosity induces Arp2/3-dependent actin remodeling, enhances NHE1 activity, and promotes hMSC spreading via upregulation of integrin-linked kinase. The resulting increase in membrane tension triggers the activation of transient receptor potential cation vanilloid 4 to facilitate calcium influx, thereby stimulating RhoA/ROCK and driving YAP-dependent RUNX2 translocation to the nucleus, leading to osteogenic differentiation. hMSCs on soft gels at elevated relative to basal viscosity favor an M2 macrophage phenotype. This study establishes fluid viscosity as a key physical cue that imprints osteogenic memory in hMSCs and promotes an immunosuppressive phenotype.**

## INTRODUCTION

Human mesenchymal stem cells (hMSCs) are stroma cells present in a number of tissues, capable of differentiating and mobilizing to damaged tissues (*1*). hMSCs have been widely explored for potential clinical applications, such as endogenous tissue regeneration and treatment of bone and cartilage defects (*1*, *2*). This is mainly due to their ease of isolation, ability to self-renew, capacity to differentiate into various cell types, and their beneficial paracrine properties (*3*, *4*). hMSCs are active mechanical objects, which sense and respond to physical cues, such as stiffness and viscoelasticity. For instance, soft (≤2 kPa) and stiff (≥10 kPa) substrates bias hMSCs toward adipogenic and osteogenic differentiation, respectively (*5*–*7*). However, natural extracellular matrix (ECM) and living tissues are not purely elastic but viscoelastic, displaying stress relaxation over different characteristic timescales [half-time ($t_{1/2}$)] (*8*–*10*). Three-dimensional (3D) fast relaxing ($t_{1/2}$ = 60 s) relative to slow relaxing gels ($t_{1/2}$ = 2300 s) of 9 to 17 kPa promote hMSC osteogenic differentiation (*10*).

To date, the majority of the cell functional assays using hMSCs have been carried out in culture media with a viscosity close to that of water (0.77 cP). Yet, the fluid viscosity in tissues is markedly elevated. Specifically, the viscosity of the interstitial fluid is in the range of 2 to 3.5 cP (*11*, *12*) and can be further increased at tumor sites due to elevated degradation of ECM, which results in macromolecular crowding (*13*). Moreover, the viscosity of whole blood in healthy human subjects varies between 4 and 6 cP (*14*) and can reach 8 cP in certain disease conditions (*15*). We recently identified extracellular fluid viscosity as a key physical cue that alters intracellular signaling pathways and counterintuitively promotes cancer cell dissemination in vitro and in vivo (*16*). Although a few studies have examined the effect of extremely high viscosity values (≥68.4 cP) on hMSC differentiation (*17*–*19*), achieving these values requires the addition of large amounts of macromolecules, which is expected to increase osmolarity. Consequently, it remains unclear whether the observed effects on hMSC differentiation are due to the extremely high viscosity values or are an indirect result of osmotic shock. Thus, it is unknown how elevated, albeit physiologically relevant, levels of fluid viscosity regulate hMSC function. The interplay between extracellular fluid viscosity and substrate stiffness or viscoelasticity has yet to be explored. Key fundamental questions with potential translational impact remain unanswered, including the following: (i) How do hMSCs differentiate when exposed to elevated viscosity on soft and stiff substrates? (ii) How do hMSCs sense the physical cue of extracellular fluid viscosity? (iii) Does elevated viscosity alter the cell phenotype and the underlying mechanisms of cell differentiation? (iv) Does the cell cytoskeleton cooperate with ion transporters and mechano/osmo-sensitive ion channels (MOSICs) to bias hMSC differentiation at elevated viscosities? (v) What is the interplay between substrate stiffness or viscoelasticity and fluid viscosity in hMSC differentiation process? (vi) How does hMSC exposure to elevated fluid viscosity affect immune cell function? We herein demonstrate that although soft substrates induce an adipogenic phenotype under basal viscosity (0.77 cP), elevated fluid viscosity promotes osteogenic differentiation. We unveil the underlying molecular mechanism of this process and also decipher how fluid viscosity alters hMSC behavior on substrates of prescribed viscoelasticity. We further establish that elevated fluid viscosity imprints mechanomemory to hMSCs. Viscosity preconditioned hMSCs promote M2 macrophage polarization.

[1]Department of Chemical and Biomolecular Engineering, Johns Hopkins University, Baltimore, MD 21218, USA. [2]Institute for NanoBioTechnology, Johns Hopkins University, Baltimore, MD 21218, USA. [3]Department of Biomedical Engineering, Johns Hopkins University, Baltimore, MD 21218, USA. [4]Deparment of Materials Science and Engineering, Johns Hopkins University, Baltimore, MD 21218, USA. [5]Department of Oncology, Sidney Kimmel Comprehensive Cancer Center, Baltimore, MD 21231, USA.
*Corresponding author. Email: konstant@jhu.edu
†These authors contributed equally to this work.
‡These authors contributed equally to this work.

## RESULTS

### Elevated extracellular fluid viscosity favors hMSC osteogenic differentiation on soft substrates

It is well established that hMSCs plated on soft substrates undergo adipogenic differentiation at a basal (0.77 cP) medium viscosity (*5*–*7*). To investigate the effects of increased extracellular fluid viscosity on hMSC function, we added prescribed amounts of methylcellulose

(65 kDa) (*16*) to hMSC cell culture medium promoting either adipogenic or osteogenic differentiation (*5*) to generate media with viscosities of either 0.77 or 8 cP (*16*). Using a freezing point depression osmometer, we verified that addition of methylcellulose did not alter the osmolarity of the media (fig. S1A). Next, hMSCs were cultured on either soft (600 Pa) or stiff (100 kPa) polyacrylamide (PA) gels (fig. S1, B and C) coated with collagen type I (*20*) and incubated with the aforementioned cell media either at basal (0.77 cP) or high (8 cP) viscosity for 6 days, with media being changed every 2 days. Notably, no alterations in PA gel stiffness were detected following submersion in media of elevated viscosity for 6 days (fig. S1D).

Consistent with prior work (*5*), hMSCs cultured on soft or stiff substrates at 0.77 cP undergo adipogenic or osteogenic differentiation, respectively, as shown by the differential regulation of adipogenic [peroxisome proliferator–activated receptor γ (PPARγ)] and osteogenic [RUNX2 and alkaline phosphatase (ALP)] markers via quantitative polymerase chain reaction (qPCR) (Fig. 1, A to C). hMSCs exposed to 8 cP assume an osteogenic phenotype even on soft gels, as evidenced by the down-regulation of PPARγ and concomitant up-regulation of RUNX2 and ALP gene expression (Fig. 1, A to C). The viscosity-induced shift from adipogenic to osteogenic phenotype was further confirmed by immunofluorescence analysis showing reduced levels of the adipogenic marker (PPARγ) in the nucleus of hMSCs on soft gels at 8 cP relative to a medium viscosity of 0.77 cP (Fig. 1, D and E). Low nuclear levels of PPARγ were observed in stiff gels irrespective of the extracellular fluid viscosity (Fig. 1, D and E). As a further validation, hMSCs display a reduced lipid droplet area at elevated than basal viscosity on soft substrates, as assessed by BODIPY 493/503 staining (Fig. 1, F and G). Consistent with this observation, reduced lipid droplet areas were detected for cells on stiff substrates regardless of the viscosity (Fig. 1, F and G). Along these lines, immunostaining showed increased nuclear levels of the osteogenic marker RUNX2 (*7*) in cells on soft gels at elevated relative to basal viscosity and on stiff gels at either viscosity (Fig. 1, H and I). These findings were replicated using hMSCs from a different donor (AllCells; fig. S1, E and F). RUNX2 nuclear translocation was detected on soft (600 Pa) gels at viscosity values as low as 4 cP and increased with increasing fluid viscosity (fig. S1G). The viscosity-induced osteogenic differentiation on soft gels was also corroborated by histological staining of ALP and von Kossa, which detect ALP activity and cell mineralization, respectively (fig. S1, H and I). Elevated viscosity induced adipogenic-to-osteogenic transdifferentiation in IMDM-containing media lacking differentiation cues (fig. S1, J and K).

In view of prior work showing that yes-associated protein (YAP) translocation to the nucleus correlates with osteogenic differentiation (*5*, *21*), we also found that elevated viscosity induced YAP nuclear entry from the cell cytoplasm in cells on soft surfaces (Fig. 1, J and K). Collectively, these data show that extracellular fluid viscosity alters hMSC fate on soft substrates. The osteogenic phenotype assumed by hMSCs on soft substrates in the presence of elevated viscosity was retained for at least 9 days after switching the medium back to 0.77 cP (fig. S1, L to N). These data illustrate that fluid viscosity imprints mechanomemory to hMSCs.

## Extracellular fluid viscosity alters morphological features of hMSCs on soft substrates

Because fluid viscosity induced a significant shift from adipogenic to osteogenic phenotype, we next wished to quantify cell morphological changes in response to viscosity at prescribed stiffness across cell populations (*22*). hMSCs, after being cultured for 6 days on soft or stiff PA gels at either 0.77 or 8 cP, were fixed and stained with phalloidin (F-actin) and Hoechst (nucleus) (*22*). Cell and nuclear boundaries were segmented on the basis of the phalloidin and Hoechst fluorescence, from which we quantified eight key morphological features: cell area, normalized actin intensity, cell major axis length, cell form factor (analogous to circularity), cell perimeter, cell eccentricity (describing the deviation from a perfect circle), cell solidity (degree of concavity), and nuclear area. Quantification of these eight parameters revealed that hMSCs cultured on soft gels at elevated viscosity are morphologically similar to cells on stiff substrates at either viscosity, whereas they are markedly different from cells on soft substrates at basal viscosity (Fig. 2, A to H). The stiffness and viscosity-mediated differences in hMSC morphology were also illustrated by Uniform Manifold Approximation and Projection (UMAP) which condenses the aforementioned eight features into a 2D space (fig. S2A). *K*-means clustering based on a silhouette score (fig. S8) identified six morphological clusters with unique cellular and nuclear features (Fig. 2I). Specifically, hMSCs on stiff gels irrespective of viscosity were primarily found in clusters C4, C5, and C6, which are also abundant in hMSCs on soft gels at elevated viscosity (Fig. 2, M to O). The cellular and nuclear morphological parameters were projected onto the UMAP space (fig. S2B) and directly compared using radar and bar plots (figs. S2C and S3). Cells in clusters C4, C5, and C6 displayed notably higher cell area, higher actin intensity, higher cell perimeter, longer axis length, higher nuclear area as well as lower form factor and solidity (figs. S2, B and C, and S3). To the contrary, cells in clusters C2 and C3, which were more prevalent in hMSCs on soft substrates at basal viscosity (Fig. 2K, L), displayed the reverse morphological characteristics (e.g., higher form factor and cell solidity and lower cell area, perimeter, and axis length) (figs. S2, B and C, and S3).

## Fluid viscosity promotes osteogenic differentiation on soft substrates via an Arp2/3-NHE1-ILK-TRPV4-RhoA-YAP–dependent pathway

We next aimed to delineate the molecular pathway mediating the adipogenic-to-osteogenic differentiation of hMSCs on soft gels in response to elevated extracellular fluid viscosity. Prior work albeit in cancer cells revealed that Arp2/3-mediated actin remodeling is a direct cell response to elevated viscosity and responsible for the formation of a dense actin network to counteract the increased viscous forces (*16*). Because fluid viscosity also induced a denser actin network in hMSCs characterized by a higher number of and longer stress fibers (Fig. 3, A to C), we examined the role of Arp2/3 in hMSC differentiation. Use of the Arp2/3-specific inhibitor CK666 (100 μM) decreased the extent of nuclear-to-cytosolic localization of the osteogenic markers RUNX2 and YAP in hMSCs cultured on soft gels at 8 cP down to the levels observed at basal viscosity (Fig. 3D and fig. S4, A and B). The role of actin remodeling in the viscosity-induced adipogenic-to-osteogenic differentiation was further validated by treating hMSCs with low levels of latrunculin A (500 nM), which partially disrupt the actin network. This intervention was sufficient to block the nuclear translocation of RUNX2 in response to fluid viscosity on soft gels and on stiff gels regardless of viscosity (fig. S4C).

We have previously demonstrated that viscosity-induced Arp2/3-dependent actin remodeling promotes Na+/H+ exchanger 1 (NHE1)

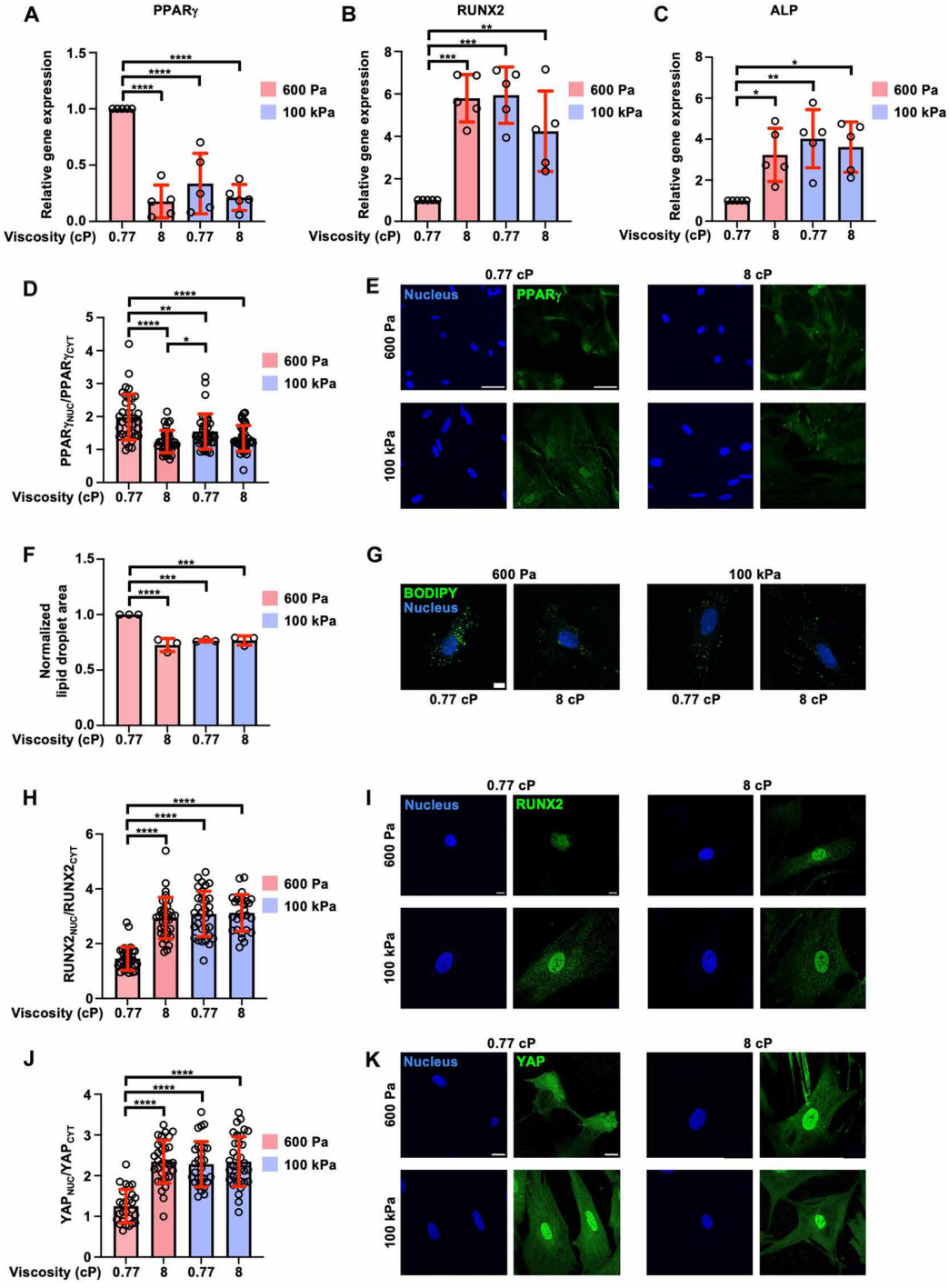


**Fig. 1. Elevated extracellular fluid viscosity promotes hMSC osteogenic differentiation on soft substrates.** In all experiments, hMSCs were plated on 2D collagen I–coated PA gels of 600 Pa or 100 kPa and cultured for 6 days in adipogenic/osteogenic inducing medium of prescribed viscosity. (**A** to **C**) Quantification of PPARγ (A), RUNX2 (B), and ALP (C) mRNA expression via qPCR. Data represent mean ± SD from five independent experiments. (**D** and **E**) Nuclear-to-cytosolic ratio of PPARγ (D) and representative immunofluorescence images of hMSCs fixed and stained with an antibody against PPARγ (green) and Hoechst (blue) (E). Data represent mean ± SD for $n$ = 36 cells from three independent experiments. (**F** and **G**) Normalized lipid droplet area quantification (F) and representative images (G) of hMSCs fixed and stained with BODIPY 493/503 (green) and with Hoechst (blue). Data represent mean ± SD from the average values of three independent experiments. (**H** and **I**) Nuclear-to-cytosolic ratio of RUNX2 (H) and representative images (I) of hMSCs fixed and stained with an antibody against RUNX2 (green) and Hoechst (blue). Data represent mean ± SD for $n \geq 37$ cells from three independent experiments. (**J** and **K**) Nuclear-to cytosolic ratio of YAP (J) and representative images (K) of hMSCs fixed and stained with an antibody against YAP (green) and Hoechst (blue). Data represent mean ± SD for $n \geq 24$ cells from three independent experiments. *$P < 0.05$, **$P < 0.01$, ***$P < 0.001$, and ****$P < 0.0001$ by one-way analysis of variance (ANOVA) followed by Tukey's multiple comparisons test [(A) to (C), (F), (H), and (J)] after log transformation (D). Scale bars, 50 μm (E), 10 μm [(G) and (I)], or 20 μm (K).

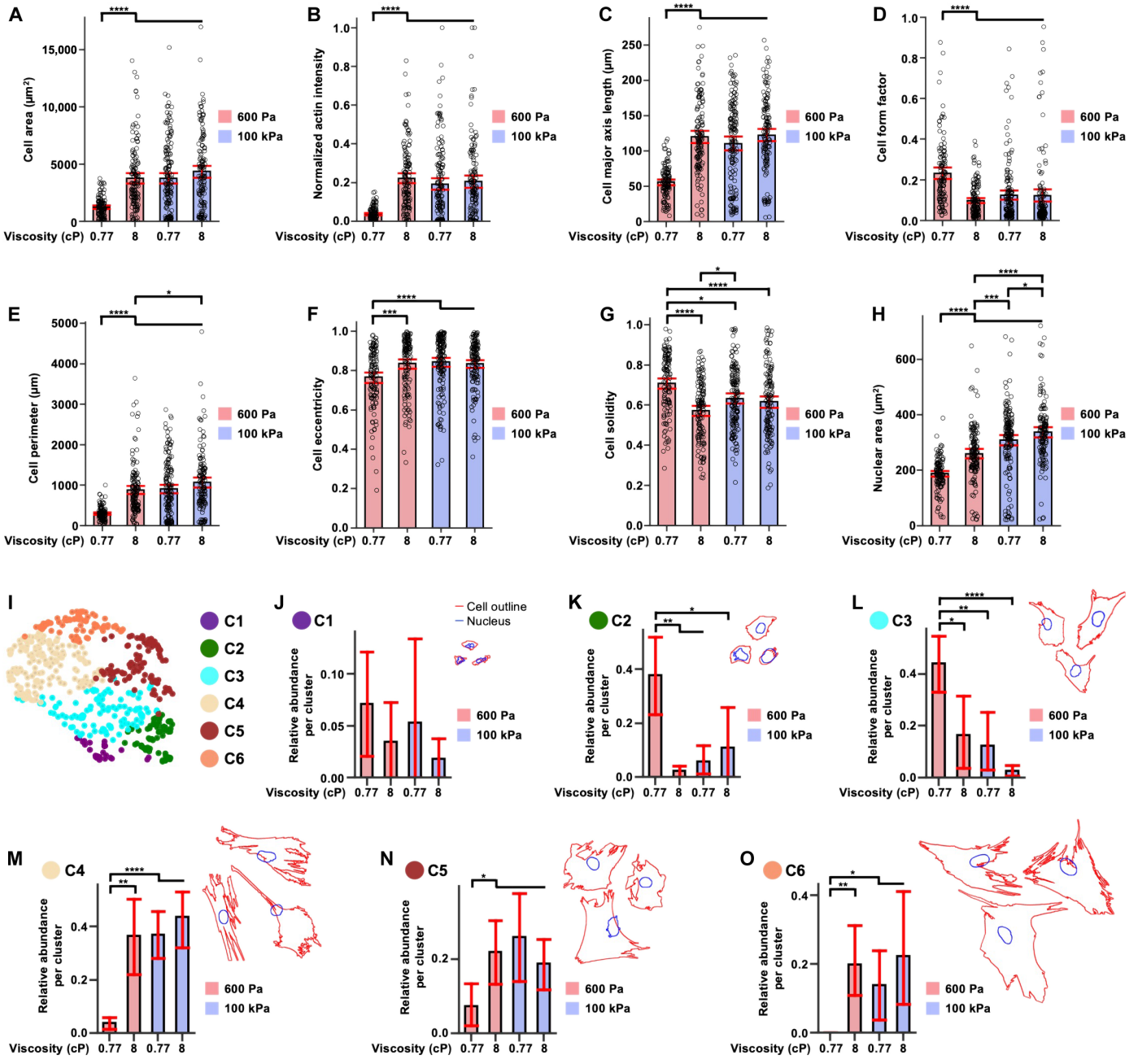


**Fig. 2. Extracellular fluid viscosity alters morphological features of hMSCs on soft substrates.** hMSCs were plated on 2D collagen I–coated PA gels of 600 Pa or 100 kPa, cultured for 6 days in adipogenic/osteogenic inducing medium of prescribed viscosity, and fixed and stained with phalloidin and Hoechst. (**A** to **H**) Bar graphs displaying the cell area (A), normalized actin intensity (B), cell major axis length (C), cell form factor (D), cell perimeter (E), cell eccentricity (F), cell solidity (G), and nuclear area (H) of hMSCs after culture for 6 days on 2D collagen I–coated soft and stiff PA gels at prescribed medium viscosity. These parameters were extracted after imaging hMSCs that were fixed and stained with phalloidin and Hoechst. Data are mean ± 95% confidence interval (CI) from $n \geq 121$ cells from three independent experiments. (**I**) Unsupervised clustering revealed six unique *k*-means morphological subtypes based on measured morphological features among hMSCs in all conditions. (**J** to **O**) Bar graphs displaying the relative abundance in each cluster (C1 to C6) of hMSCs seeded on soft or stiff gels and exposed to basal or elevated viscosity with the respective representative cellular (red) and nuclear (blue) morphologies of cells from each *k*-means cluster. Data are mean ± 95% CI from $n \geq 121$ cells from the average values of three technical repeats of three independent experiments. *$P < 0.05$, **$P < 0.01$, ***$P < 0.001$, and ****$P < 0.0001$ by one-way ANOVA [(A) to (H) and (J) to (O)].

localization to the plasma membrane and increases NHE1 activity in breast cancer cells (*16*). In line with these findings, we herein observed that elevated fluid viscosity markedly increased NHE1 activity in hMSCs cultured on soft substrates without affecting NHE1 expression (Fig. 3E and fig. S4D). NHE1 is known to increase cell volume via water uptake (*23*). NHE1-dependent cell swelling leads to increased membrane tension (*16*). Consistent with this notion, hMSCs on soft gels at elevated viscosity exhibited increased membrane tension, as probed by the use of the live-cell membrane tension probe Flipper-TR in conjunction with fluorescence lifetime imaging microscopy (FLIM)

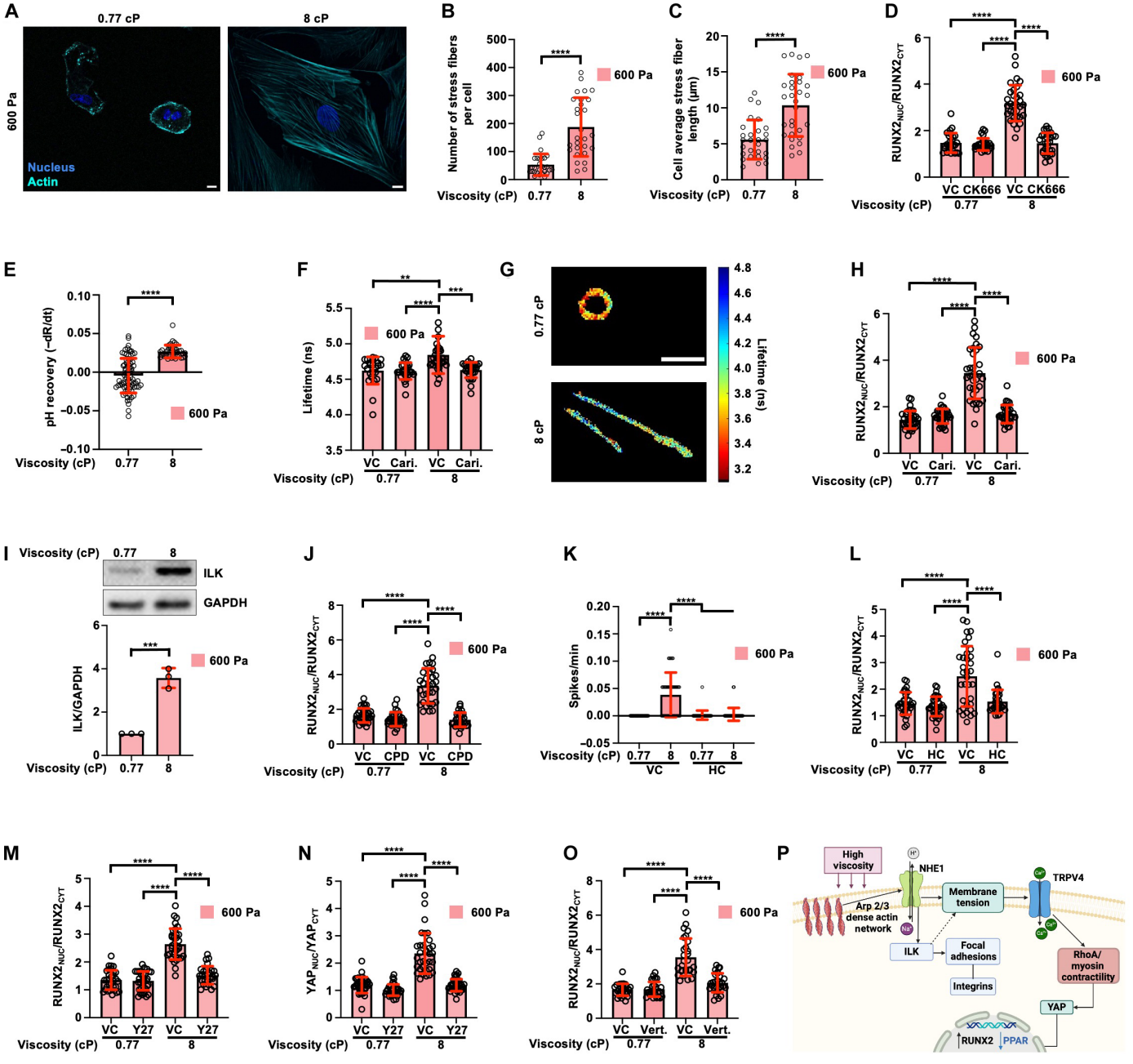


**Fig. 3. Fluid viscosity promotes osteogenic differentiation on soft substrates via an Arp2/3-NHE1-ILK-TRPV4-RhoA-YAP-dependent pathway.** In all experiments, hMSCs were plated on 2D collagen I–coated PA gels of 600 Pa and cultured for 6 days in adipogenic/osteogenic inducing medium of prescribed viscosity in the presence or absence of specific inhibitors. (**A** to **C**) Representative images (A), number of stress fibers per cells (B), and cell average stress fiber length (C) of hMSCs fixed and stained with phalloidin (cyan) and Hoechst (blue). (**D**) Nuclear-to-cytosolic ratio of RUNX2 in hMSCs incubated with CK666 or vehicle control (VC). (**E**) Measurement of NHE1 activity using a $NH_4Cl$ prepulse technique by quantifying the rate of pH recovery of hMSCs loaded with pHrodo. (**F** and **G**) Flipper-TR lifetime quantification of membrane tension (F) and representative images (G) of hMSCs treated with cariporide (Cari.) or VC. (**H**) Nuclear-to-cytosolic ratio of RUNX2 in hMSCs incubated with cariporide or VC. (**I**) Representative Western blot images of ILK and quantification of protein expression. (**J**) Nuclear-to-cytosolic ratio of RUNX2 in hMSCs incubated with CPD22 or VC. (**K** and **L**) Fluo-4 AM spikes/min (K) and nuclear-to-cytosolic ratio of RUNX2 (L) in hMSCs incubated with the TRPV4 inhibitor HC060747 or VC. (**M** to **O**) Nuclear-to-cytosolic ratio of RUNX2 [(M) and (O)] and YAP (N) incubated with Y-27632 [(M) and (N)] or verteporfin (O) or VC. (**P**) Proposed pathway by which fluid viscosity induces osteogenic differentiation on soft gels (figure generated with BioRender.com/z75q476). Data represent mean ± SD for $n \geq 28$ [(A) to (C) and (I)], ≥26 [(D) and (F)], ≥39 [(E) and (K)], ≥33 (H), ≥32 (L), and ≥31 [(M) to (O)] cells from three independent experiments. $^{**}P < 0.01$, $^{***}P < 0.001$, and $^{****}P < 0.0001$ by unpaired *t* test [(B), (C), and (I)], Kruskal-Wallis test followed by Dunn's multiple comparisons [(D), (F), (K), and (N)], Mann-Whitney test (E), and one-way ANOVA followed by Tukey's multiple comparisons test [(L), (M), and (O)] after log transformation [(J) and (H)]. Scale bars, 10 μm (A) and 90 μm (G). GAPDH, glyceraldehyde phosphate dehydrogenase.

(Fig. 3, F and G). Use of the selective NHE1 inhibitor, cariporide (10 μM), abrogated the viscosity-induced increase in membrane tension of hMSCs as well as the nuclear-to-cytosolic RUNX2 localization down to the levels observed at basal viscosity (Fig. 3, F and H). Similar changes in RUNX2 nuclear localization were observed using an alternative NHE1 inhibitor, 5-[N-ethyl-N-isopropyl] amiloride (EIPA) (20 μM) (fig. S4E). Cumulatively, these findings illustrate the critical roles of Arp2/3-dependent actin remodeling and NHE1 activity in adipogenic-to-osteogenic shift induced by elevated viscosity on soft substrates.

Integrin linked kinase (ILK) is a pseudokinase, which also acts as a scaffold that links integrins to the actin cytoskeleton (*24*). In light of our findings showing that hMSCs on soft surfaces at elevated relative to basal viscosity displayed a larger cell area and a denser actin network (fig. S2A and Fig. 3, A to C), we examined the potential involvement of ILK in viscosity-mediated hMSC transdifferentiation. First, ILK protein expression was ~4-fold up-regulated in hMSCs on soft substrates at 8 cP as opposed to 0.77 cP (Fig. 3I). This ILK up-regulation was abrogated upon inhibition of NHE1 activity via cariporide (10 μM) (fig. S4F), suggesting that NHE1 is upstream of ILK. ILK inhibition using CPD22 (*25*) blocked RUNX2 translocation to the nucleus in hMSCs on soft gels at 8 cP down to the basal viscosity levels (Fig. 3J), thereby preventing osteogenic differentiation. Notably, ILK inhibition had no effect on the nuclear-to-cytosolic RUNX2 localization in hMSCs cultured on soft gels at 0.77 cP relative to vehicle control (Fig. 3J). As expected, ILK inhibition also reduced the cell spreading area and the cell major axis length (fig. S4, G to I).

Changes in membrane tension trigger the activation of MOSICs via a conformational change which causes MOSIC gates to open and allow ion influx (*26*). Consistent with the viscosity-mediated increase of hMSC membrane tension (Fig. 3, F and G), viscosity induced calcium flashes in cells on soft gels at elevated relative to basal viscosity (Fig. 3K and fig. S4J). In accord with prior work on breast cancer cells showing that fluid viscosity activates the transient receptor potential cation vanilloid 4 (TRPV4) (*16*), inhibition of TRPV4 via HC-067047 (5 μM) abolished the viscosity-mediated calcium flashes in cells on soft gels at 8 cP while having no effect at 0.77 cP (Fig. 3K). The viscosity-induced calcium flashes were also abrogated by inhibiting NHE1 or ILK (fig. S4K), suggesting that they are upstream regulators of TRPV4. Moreover, TRPV4 inhibition suppressed the viscosity-induced translocation of both RUNX2 and YAP to the nucleus (Fig. 3L and fig. S4, L and M), thereby illustrating the critical role of TRPV4 in viscosity-mediated adipogenic-to-osteogenic differentiation. In line with prior work showing that TRPV4-dependent calcium influx triggers RhoA/ROCK activation (*16*), inhibition of ROCK via Y27632 (10 μM) in hMSCs on soft gels at 8 cP suppressed the nuclear-to-cytosolic ratio of YAP and RUNX2 down to the levels detected at 0.77 cP (Fig. 3, M and N). These findings implicate RhoA/ROCK activation in hMSC osteogenic differentiation in response to fluid viscosity. Because YAP inhibition by verteporfin (0.1 μM) (*16*, *27*) or K975 (5 μM) (*28*) interferes with RUNX2 translocation to the nucleus at elevated viscosity (Fig. 3O and fig. S4N), we postulate that YAP regulates the spatial localization of RUNX2.

Together, we demonstrate that elevated extracellular viscosity induces the formation of a dense Arp2/3-dependent actin network (Fig. 3, A to C) that promotes NHE1 localization to the plasma membrane (*16*) and increases NHE1 activity (Fig. 3E). Viscosity-induced NHE1-dependent swelling (*16*, *23*) and ILK-mediated cell spreading increase hMSC membrane tension, which in turn triggers the activation of TRPV4 to promote calcium influx, thereby stimulating the RhoA/ROCK pathway and driving YAP translocation to the nucleus (Fig. 3P). YAP facilitates the nuclear translocation of RUNX2, thus promoting hMSC adipogenic-to-osteogenic differentiation on soft substrates in response to fluid viscosity (Fig. 3P).

### Fluid viscosity regulates hMSC fate on substrates of prescribed stiffness and stress relaxation

Natural ECM and living tissues are viscoelastic exhibiting different stress relaxation $t_{1/2}$ (*8*, *10*) that vary from 60 s (fast-relaxing) to >1000 s (slow-relaxing; approaching elastic) (*29*). In addition to substrate stiffness, viscoelasticity alters hMSC function (*10*). We thus aimed to investigate the interplay of substrate viscoelasticity and fluid viscosity on hMSC function. Viscoelastic 1-kPa PA gels of prescribed stress relaxation times (fig. S5, A and B) were prepared by introducing linear acrylamide (LA) chains into the acrylamide and bis-acrylamide mixture (*30*). In line with our findings using purely elastic (0.6 kPa) gels (Fig. 1), elevated viscosity induced hMSC adipogenic-to-osteogenic differentiation in slow relaxing soft gels (1 kPa and $t_{1/2}$ = 1366 s), as evidenced by enhanced translocation of RUNX2 to the nucleus (Fig. 4, A and B). hMSCs on fast ($t_{1/2}$ = 157 s) relative to slow relaxing soft gels at basal viscosity exhibited a twofold higher nuclear-to-cytosolic RUNX2 ratio, which is indicative of an osteogenic phenotype (Fig. 4, A and B). Elevated viscosity further increased, albeit moderately, RUNX2 nuclear translocation on fast relaxing gels (Fig. 4, A and B). The observed hMSC phenotypes were further substantiated by cell morphological analysis showing that hMSCs on slow relaxing gels at basal viscosity are morphologically markedly distinct from the three other conditions in terms of cell area, major axis length, eccentricity, solidity, form factor, and cell perimeter (fig. S5, C to H). Our findings are in line with previous data showing that osteosarcoma (*31*) and myoblasts (*32*) spread more on fast relative to slow relaxing soft (1.4 to 2.8 kPa) gels.

Osteosarcoma cells display the reverse spreading pattern at fast and slow relaxing gels of higher stiffness (3.4 and 9 kPa). In view of these prior findings showing differences in osteosarcoma cell spreading within a narrow stiffness window, we next aimed to identify the lowest stiffness threshold at which adipogenic-to-osteogenic hMSC transdifferentiation occurs at basal viscosity. A stiffness of 4 kPa is sufficient to induce an osteogenic phenotype in hMSCs at 0.77 cP (fig. S6A). In light of these observations, we next wished to examine how fluid viscosity alters hMSC lineage on 4-kPa gels of prescribed viscoelasticity. In line with our data using purely elastic PA gels, hMSCs on slow ($t_{1/2}$ = 1179 s) relaxing 4-kPa gels exhibited a high nuclear-to-cytosolic RUNX2 ratio, indicative of an osteogenic phenotype (Fig. 4, C and D). hMSCs on fast ($t_{1/2}$ = 239 s) relative to slow ($t_{1/2}$ = 1179 s) relaxing 4-kPa gels at basal viscosity displayed a threefold lower RUNX2 nuclear translocation that is consistent with an adipogenic phenotype (Fig. 4, C and D). Moreover, these cells spread less (fig. S6, D to I), which is in concert with previous work using osteosarcoma cells (*31*). hMSCs on fast relaxing 4-kPa gels albeit at elevated viscosity displayed an osteogenic phenotype, as assessed by the RUNX2 nuclear-to-cytosolic ratio and morphological parameters (Fig. 4, C and D, and fig. S6, D to I), and were morphologically similar to hMSCs on slow relaxing gels at either viscosity (fig. S6, D to I). Similar trends for the RUNX2 nuclear-to-cytosolic ratio were also observed for hMSCs on fast ($t_{1/2}$ = 100 s) and slow ($t_{1/2}$ = 2400 s) relaxing alginate-based gels (*10*, *29*, *31*) of 20 kPa (fig. S7, A to D). Notably, the differences in the RUNX2 nuclear-to-cytosolic

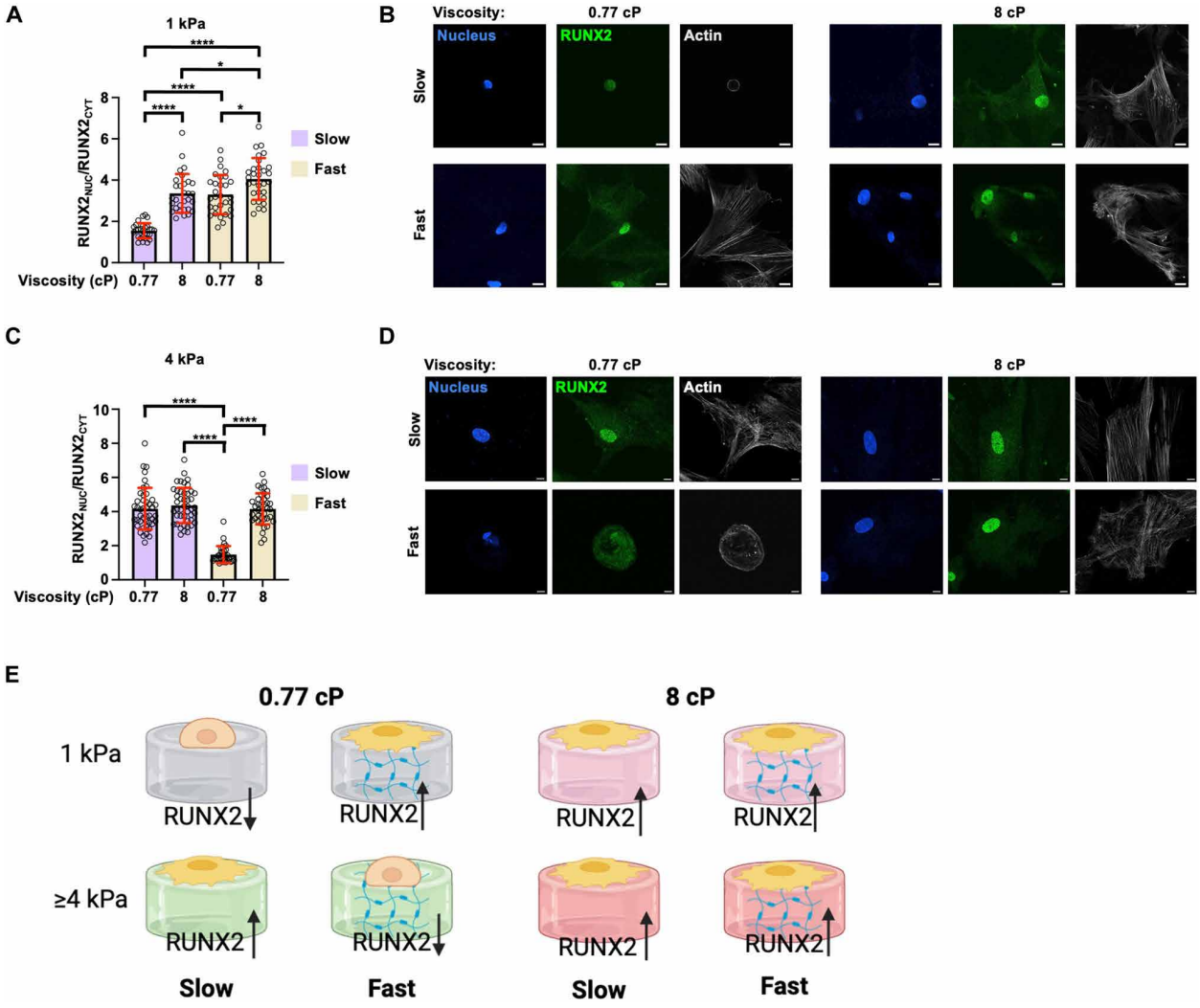


**Fig. 4. Fluid viscosity regulates hMSC fate on substrates of prescribed stiffness and stress relaxation.** In all experiments, hMSCs were cultured for 6 days on 2D collagen I–coated, slow, and fast relaxing gels of prescribed stiffness at specified viscosities. (**A** and **B**) Nuclear-to-cytosolic ratio of RUNX2 (A) and representative immunofluorescence images of hMSCs fixed and stained with an antibody against RUNX2 (green), Hoechst (blue), and phalloidin (white) (B). Data represent mean ± SD for $n \geq 28$ cells from three independent experiments. (**C** and **D**) Nuclear-to-cytosolic ratio of RUNX2 (C) and representative immunofluorescence images of hMSCs fixed and stained with an antibody against RUNX2 (green), Hoechst (blue), and phalloidin (white) (D). Data represent mean ± SD for $n \geq 32$ cells from three independent experiments. (**E**) Schematic summarizing RUNX2 localization in viscoelastic gels in the presence or absence of elevated viscosity (figure generated with BioRender.com/g74o356). *$P < 0.05$ and ****$P < 0.0001$ by one-way ANOVA followed by Tukey's multiple comparisons test after log transformation (A) or Kruskal-Wallis test followed by Dunn's multiple comparisons (C). Scale bars, 10 μm [(B) and (D)].

ratio were less pronounced at 20-kPa alginate-based gels relative to 4-kPa PA gels (fig. S7C), which is possibly attributed to the higher substrate stiffness that promotes more spreading and/or the presence of different adhesion ligands [i.e., Arg-Gly-Asp (RGD) versus collagen I]. In summary, our data reveal that extracellular viscosity is sufficient to induce adipogenic-to-osteogenic transdifferentiation at prescribed stiffness or viscoelasticity (Fig. 4E).

## hMSCs cultured on soft substrates in the presence of elevated or basal viscosity promote distinct macrophage phenotypes

MSCs have been tested for potential cell therapies due to their ability to produce cytokines, growth factors, and metabolic by-products that regulate the behavior of various immune cells, including macrophages (*33*–*36*). Prior work has shown that MSCs cultured on stiff substrates had higher immunosuppressive properties (*37*, *38*). Moreover, conditioned media from hMSCs cultured on stiffer substrates (64 versus 0.2 kPa) biased macrophage polarization toward an M2 phenotype (*35*). Considering these previous findings, we examined whether the cytokine secretion profile of hMSCs cultured on soft substrates at elevated viscosity differed from that at basal viscosity. The conditioned medium collected from hMSCs pretreated at 8 cP as opposed to 0.77 cP contained higher levels of M2 macrophage–polarizing cytokines, including Chemokine (C-C motif) ligand 2/monocyte chemoattractant protein 1 (CCL2/MCP1) (*39*), interleukin-6 (IL-6) (*40*), IL-8 (*40*), and IL-10 (*40*), and reduced levels of M1-promoting cytokines, such as C-X-C motif chemokine ligand 10/Interferon gamma-induced protein 10 (CXCL10/IP-10) (*41*, *42*)

and IL-1β/IL-1F2 (Fig. 5A) (*43*). Increasing trends were also observed for additional M2-polarizing cytokines [CXCL12/Stromal cell-derived factor 1 (SDF-1) (*44*), IL-4 (*40*), IL-17A (*45*), and Macrophage migration inhibitory factor (MIF) (*46*)] (Fig. 5A).

Building on these data, we also observed that hMSCs cultured on soft (600 Pa) gels at elevated viscosity or stiff (100 kPa) substrates at either viscosity preferentially induced M2 macrophage polarization. This was substantiated by the up-regulation of M2-specific markers [Arginase 1, PPARγ, and mannose receptor C-type 1 (MRC1)] and down-regulation of M1-specific markers [inducible nitric oxide synthase (iNOS)] (Fig. 5, B to E). We further validated these qPCR measurements with immunofluorescence assays which revealed increased levels of PPARγ and MRC1 in macrophages treated with conditioned media from hMSCs on stiff substrates at either viscosity or on soft gels at 8 cP (Fig. 5, F to I). Moreover, elevated viscosity-mediated up-regulation of Arginase 1 (an M2 marker) was observed by immunofluorescence and Western blotting analysis (Fig. 5, J to L). Cumulatively, these data suggest that elevated viscosity promotes the immunosuppressive potential of hMSCs on soft substrates.

## DISCUSSION

This work establishes extracellular fluid viscosity as a key physical cue that regulates hMSC differentiation and function in substrates of prescribed stiffness and viscoelasticity. A recent study revealed that fluid viscosity, albeit only at very high levels (21.8 or 68.1 cP), increases the percentage of osteogenesis on stiff (21 kPa) surfaces (*19*). Notably, media of such high viscosities exhibit increased

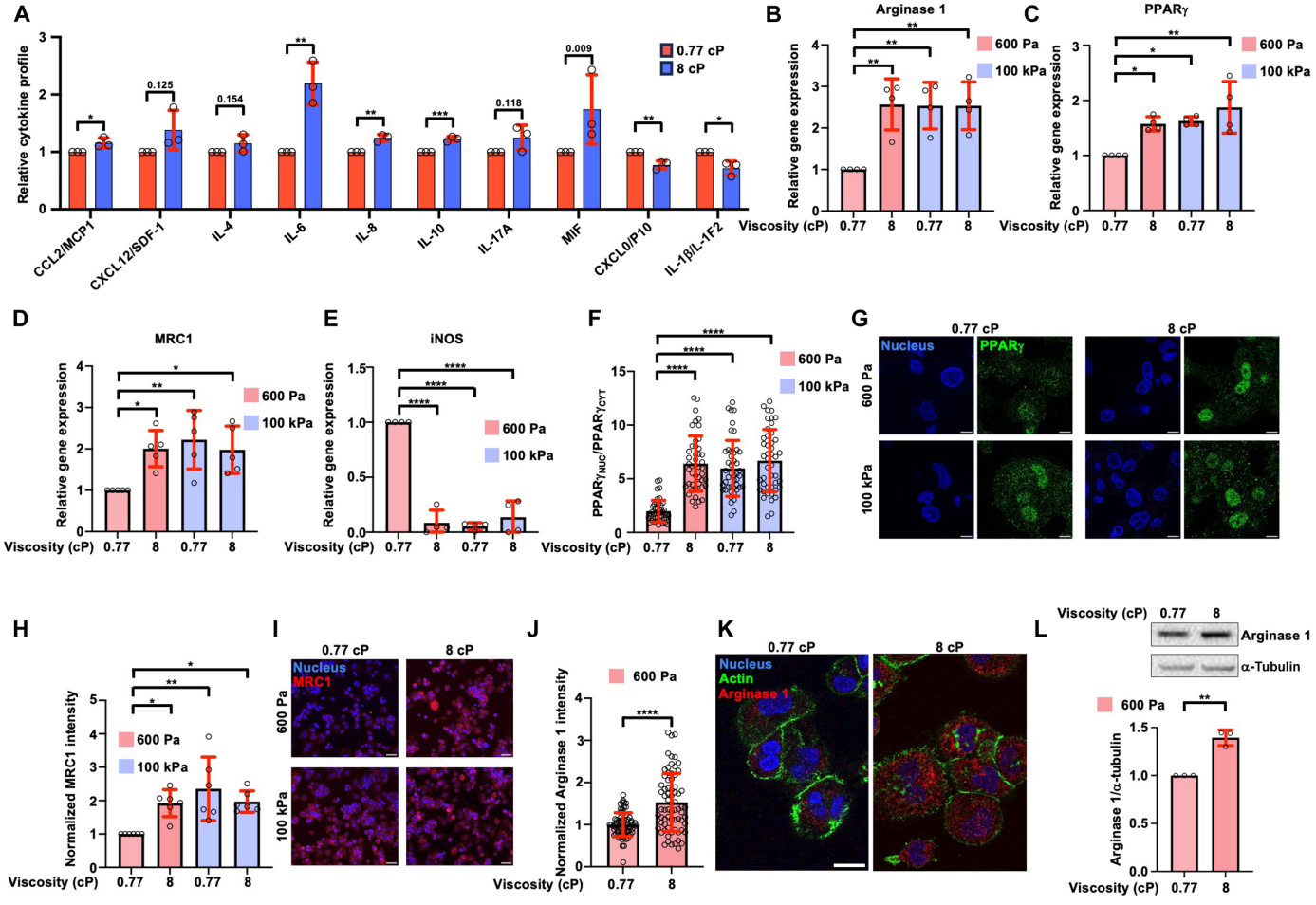


**Fig. 5. hMSCs cultured on soft substrates in the presence of elevated or basal viscosity promote distinct macrophage phenotypes.** (**A**) Quantification of RPMI-conditioned media collected from hMSCs cultured on soft substrates (600 Pa) following their pretreatment at prescribed viscosity. Data represent mean ± SD from three independent experiments. In all subsequent experiments, M0 macrophages were incubated for 2 days with RPMI-conditioned media collected from hMSCs cultured on soft or stiff substrates following their pretreatment at prescribed viscosity. (**B** to **E**) Quantification of Arginase 1 (B), PPARγ (C), MRC1 (D), and iNOS (E) mRNA expression via qPCR. Data represent mean ± SD from $n \geq 3$ independent experiments. (**F** and **G**) Nuclear-to-cytosolic ratio of PPARγ (F) and representative immunofluorescence images of macrophages fixed and stained with an antibody against PPARγ (green) and Hoechst (blue) (G). Data represent mean ± SD for $n = 45$ cells from three independent experiments. (**H** and **I**) Quantification (H) and representative images (I) of MRC1 (red) macrophage intensity normalized to Hoechst (blue). Data represent mean ± SD of two frames per condition from three independent experiments. (**J** and **K**) Quantification (J) and representative images (K) of Arginase1 macrophage intensity normalized to the baseline viscosity control. Data represent mean ± SD for $n = 71$ cells from three independent experiments. (**L**) Representative WB images and quantification of Arginase1 protein expression. Data are mean ± SD from three independent experiments. *$P < 0.05$, **$P < 0.01$, ***$P < 0.001$, and ****$P < 0.0001$ by unpaired *t* test [(A), (J), and (L)] or one-way ANOVA followed by Tukey's multiple comparisons test [(B) to (E) and (H)] after log transformation (F). Scale bars, 10 μm (G), 20 μm (K), or 50 μm (I).

osmolarities, thereby making it challenging to decouple the effects of high viscosity from high osmolarity on hMSC differentiation. Also, given that this high stiffness (21 kPa) normally promotes an osteogenic phenotype (*5*), we chose to assess the effect of physiologically relevant levels of fluid viscosity on hMSCs cultured on soft and stiff surfaces. We herein demonstrated that fluid viscosity is sufficient to induce osteogenic differentiation on soft gels. Using a high-throughput data science approach based on principal components analysis and UMAP visualization, we also showed that this transdifferentiation process was accompanied by marked hMSC morphological changes that are consistent with this phenotypic shift. We elucidated the signaling cascade by which elevated fluid viscosity biases hMSCs toward osteogenic differentiation, by focusing on the cross-talk between the cell cytoskeleton, ion transporters, and MOSICs. Specifically, different cytoskeletal players, involving Arp2/3-dependent actin remodeling, integrin-linked kinase, and Rho/ROCK contractility, coordinate with the ion transporter NHE1 and the MOSIC TRPV4 to regulate hMSC fate via YAP-dependent RUNX2 translocation to the nucleus. By using viscoelastic PA and alginate-based gels, we extended our findings and revealed that at prescribed stiffness and stress relaxation $t_{1/2}$ where an adipogenic phenotype is favored, extracellular fluid viscosity is sufficient to promote adipogenic-to-osteogenic transition. Our findings hold the potential of opening previously unexplored avenues for stem cell therapies relevant to tissue regeneration and engraftment. A key limitation in the translational application of hMSCs is their poor survival and retention of osteogenic phenotype posttransplantation (*33*). Given that elevated fluid viscosity imprints long-term osteogenic memory in hMSCs and promotes their spreading and adhesion, we postulate that viscosity preconditioning may confer hMSCs with a competitive advantage for survival at sites of engraftments. This is further substantiated by our findings that hMSC exposure to elevated fluid viscosity promotes an immunosuppressive response in macrophages, and as such, viscosity preconditioning of hMSCs may hold the potential of reducing rejection after engraftment.

## MATERIALS AND METHODS

### hMSC culture and pharmacological inhibitors

hMSCs, isolated from the human bone marrow of a female donor (Lonza), were cultured at passage 5 (P5). hMSCs were expanded and frozen in 90% fetal bovine serum (FBS; 16140071, Gibco) and 10% dimethyl sulfoxide (D2650, Sigma-Aldrich) and marked as P6. For all experiments, the same passage number of hMSCs (P6) was used. Select experiments were performed using hMSCs isolated from the human bone marrow of a different donor (AllCells) and tested at P7. Freshly thawed hMSCs were cultured in growth media consisting of α-minimum essential medium without nucleosides (1256056, Thermo Fisher Scientific), 16.7% FBS, 1% L-glutamine (25030149, Thermo Fisher Scientific), and 1% penicillin/streptomycin (P/S; 10,000 U/ml; 15140122, Gibco). The cell culture medium was changed every 2 days. When cells reached 70% confluency, they were plated on either PA or alginate gels of prescribed stiffness and viscoelasticity in growth media. Once cells adhered to the substrate, the growth medium was replaced with a 1:1 mixture of adipogenic and osteogenic inductive medium (*5*), or in select experiments with Iscove's modified Dulbecco's medium (IMDM)-containing medium lacking differentiation cues, of prescribed viscosity.

Adipogenic medium was prepared by supplementing IMDM medium (12440054_3647491561, Life Technologies) with 30% FBS, 2% P/S, insulin (40 μg/ml; I9278, Sigma-Aldrich), 4 μM dexamethasone (D1756, Sigma-Aldrich), and 2 mM 3-isobutyl-1-methylaxanthine (I5879, Sigma-Aldrich). Osteogenic medium was generated using IMDM medium supplemented with 20% FBS, 2% P/S, 400 nM dexamethasone, 200 μM ascorbic acid (49752, Sigma-Aldrich), and 80 mM β-glycerol phosphate (50020, Sigma-Aldrich). Ten milliliters of each medium was mixed together to obtain the adipogenic and osteogenic inductive mixture. To generate media with viscosities of 3, 4, 6, and 8 cP, 20 ml of 0.76, 0.90, 1.10, and 1.24% methylcellulose (HSC001, R&D Systems), respectively, in IMDM was mixed with an equal volume of adipogenic and osteogenic inductive mixture, resulting in final methylcellulose concentrations of 0.38, 0.45, 0.55, and 0.6% (*16*). Media of basal viscosity (0.77 cP) was made by adding 20 ml of IMDM to the inductive mixture. IMDM-containing media of prescribed viscosity were also generated albeit lacking adipogenic and osteogenic inductive mixture. hMSCs were cultured on hydrogels of prescribed stiffness and viscoelasticity for 6 days using the adipogenic and osteogenic inductive media of prescribed viscosity. Media was changed every 2 days. The osmolarity of the adipogenic/osteogenic induction medium at either 0.77 or 8 cP was measured by using a 3205 Single-Sample Osmometer (Advanced Instruments) (fig. S1A).

In select experiments, hMSCs were treated with the following pharmacological agents or corresponding vehicle controls for 6 days: CK666 (100 μM; SML0006, Sigma-Aldrich), latrunculin A (500 nM; L5163, Sigma-Aldrich), cariporide (10 μM; SML1360, Sigma-Aldrich), CPD22 (2.5 μM; 407331, Sigma-Aldrich), HC060747 (5 μM; 616521, Sigma-Aldrich), Y-27632 (10 μM; Y0503, Sigma-Aldrich), verteporfin (0.1 μM; SML0534, Sigma-Aldrich) ), EIPA (20 μM; A3085, Sigma-Aldrich), K975 (5 μM; HY138565, MedChemExpress), and GSK2193874 (5 μM; SML0942, Sigma-Aldrich).

### RNA extraction and qPCR analysis

Cells (20,000) were seeded onto either soft (600 Pa) or stiff (100 kPa) 22 μm–by–40 μm PA gels and cultured for 6 days in adipogenic and osteogenic inductive medium of prescribed viscosity. After 6 days, cells were washed three times with 2 ml of 1× phosphate-buffered saline (PBS) and then incubated with 3 ml of TrypLE Express Enzyme (12604013, Thermo Fisher Scientific) at 5% $CO_2$ and 37°C to induce cell detachment. Once cells were detached, 7 ml of Dulbecco's modified Eagle's medium (DMEM; 11995073, Thermo Fisher Scientific) was added to each gel, and cells were collected into 15-ml tubes and centrifuged at 0.3*g* for 5 min. Cell pellets were resuspended in 1 ml of 1× PBS and centrifuged again at 0.3*g* for 5 min. Last, cell pellets were resuspended in 150 μl of TRIzol reagent (15596026, Life Technologies) and incubated for 5 min on ice. RNA was extracted using a Direct-zol RNA Miniprep Plus kit (R2070, Zymo Research) according to the manufacturer's protocol. cDNA was generated from the extracted RNA using the Iscript cDNA Synthesis Kit (1708891, Bio-Rad) and following the manufacturer's instructions. qPCR reactions were carried out in 384-well ICycler iQ PCR plates (2239441, Bio-Rad) using the following components: 10 μl of Itaq Universal SYBR (1725122, Bio-Rad), 7 μl of DNase/RNase-free $H_2O$, 2 μl of forward and reverse primers (20 μM), and 1 μl of cDNA. The primers used are as follows: PPARγ forward sequence 5′-AGCCTGCGAAAGCCTTTTGGTG-3′ and reverse sequence 5′-GGCTTCACATTCAGCAAACCTGG-3′;

RUNX2 forward sequence 5′-ATGCTTCATTCGCCTCAC-3′ and reverse sequence 5′-ACTGCTTGCAGCCTTAAAT-3′; ALP forward sequence 5′-AGGGACATTGACGTGATCAT-3′ and reverse sequence 5′-GGCTTCACATTCAGCAAACCTGG-3′; iNOS forward sequence 5′-AGGGACAAGCCTACCCCTC-3′ and reverse sequence 5′-CTCATCTCCCGTCAGTTGGT-3′; Arginase 1 forward sequence 5′-GTGGAAACTTGCATGGACAAC-3′ and reverse sequence 5′-AATCCTGGCACATCGGGAATC-3′; MRC1 forward sequence 5′-TCCGGGTGCTGTTCTCCTA-3′ and reverse sequence 5′-CCAGTCTGTTTTTGATGGCACT-3′; 18*S* forward sequence 5′-CAGCCACCCGAGATTGAGCA-3′ and reverse sequence 5′-TAGTAGCGACGGGCGGTGTG-3′.

Three technical replicates were generated for each biological repeat. The reaction was carried out in an CFX Opus 384 Real-Time PCR Detection System (Bio-Rad) under the following conditions: 1 cycle at 95°C for 30 s; 40 cycles at 95°C for 10 s and 60°C for 30 s; and 51 cycles starting at 70°C and increasing by 0.5°C every 30 s up to 95°C.

### Immunofluorescence

PA gels were prepared in a 12- or 24-well glass-bottom plate (P12-1.5H-N or P24-1.5H-N, Cellvis), treated with sulfo-(sulfosuccinimidyl 6-(4′-azido-2′-nitrophenylamino)hexanoate) (0.5 mg/ml; 22589, Thermo Fisher Scientific) dissolved in pH-adjusted water [47.5 ml of deionized (DI) $H_2O$, 2.5 ml Hepes, and 160 μl of NaOH], and exposed to ultraviolet (UV) light for 11 min. Type I rat tail collagen (20 μg/ml; A1048301, Gibco) dissolved in pH-adjusted PBS (47.5 ml of DI PBS, 2.5 ml of Hepes, and 160 μl of NaOH) was then added to the gels and left overnight at 37°C and 5% $CO_2$. hMSCs were plated on the gels and cultured overnight in growth medium, which was then replaced by the adipogenic and osteogenic inducing medium of prescribed viscosity. In select experiments, inhibitors or their corresponding vehicle controls were added to the media. Media containing the inhibitor or vehicle control was replaced every 2 days. After 6 days of treatment, cells were washed twice with 1× PBS, then fixed with 4% paraformaldehyde (J19943K2, Thermo Fisher Scientific) for 15 min, washed twice with 1× PBS, and permeabilized for 15 min with 1% Triton X-100 (T9284, Millipore Sigma) dissolved in 1× PBS (*47*). Blocking buffer consisting of 2% bovine serum albumin (BSA; A7030, Sigma-Aldrich) and 0.1% Triton X-100 was then added to the cells for 1 hour and aspirated off before overnight cell incubation at 4°C with the following primary antibodies diluted in blocking buffer: anti-YAP1 (1:50; sc-101199, Santa Cruz Biotechnology), anti-PPARγ (1:1000; MA5-14889, Thermo Fisher Scientific), anti-RUNX2 (1:50; PCR-RUNX2-1B7,DHSB; 1:200, H00000860-M02, Thermo Fisher Scientific), anti-Arginase1 (1:100; sc-166920, Santa Cruz Biotechnology), or anti-MRC1 [1:200; MR Mab #46, Developmental Studies Hybridoma Bank (DSHB)]. Cells were washed three times with 1× PBS and incubated for 1 hour at room temperature with the following secondary antibodies and/or fluorescent molecules diluted in blocking buffer: Alexa Fluor 488 goat anti-rabbit (H+L) (1:200; A11034, Invitrogen), Alexa Fluor 488 goat anti-mouse (H+L) (1:200; A11029, Invitrogen), Alexa Fluor 568 goat anti-mouse (H+L) (1:1000; A11004, Invitrogen), Alexa Fluor Plus 647 goat anti-mouse (H+L) (1:100; A32728, Invitrogen), rhodamine phalloidin (1:1000; R415, Invitrogen), Alexa Fluor 647 phalloidin (1:1000; A22287, Thermo Fisher Scientific), and/or Hoechst 33342 (1:1000; 561908, BD Biosciences). Last, cells were washed three times with 1× PBS and imaged with a Nikon A1 or AXR confocal microscope using a Plan Apo 60×/1.4 numerical aperture (NA) (A1) or Plan Apo 40×/1.15 water immersion (WI) (AXR) objective, respectively. Images were analyzed in ImageJ. For cell immunostaining using alginate gels, instead of using regular PBS buffer, we used PBS supplemented with 2 mM calcium chloride (C7902, Sigma-Aldrich).

### PA gel fabrication

PA gels of prescribed stiffness were generated as previously described (*20*). Briefly, acrylamide (A) (40%; 1610140, Bio-Rad) and *N*,*N*-methylene bisacrylamide (B) (2%; 1610142, Bio-Rad) were mixed in DI $H_2O$ to reach the following final concentrations: 3% A/0.06% B, 3% A/0.1% B, 3% A/0.2% B, 8% A/0.07% B, 8% A/0.2% B, and 12% A/6% B, which correspond to gels with stiffness of 600 Pa, 1 kPa, 2 kPa, 4 kPa, 15 kPa, and 100 kPa, respectively. Hepes (50 mM; 15630080, Thermo Fisher Scientific) was added to each mixture. Compression tests using an E42.503 Exceed MTS Systems Corporation machine were performed to assess stiffness. The gel mixture was degassed for 20 min. Gels were polymerized using 10% ammonium persulfate (APS; 1610700, Bio-Rad) and 0.4% Tetramethylethylenediamine (TEMED) (1610801, Bio-Rad). Glass coverslips or 12- or 24-well glass-bottom plates were activated with glutaraldehyde (16360, Electron Microscopy Sciences) as previously described (*20*). The final PA solutions were placed on top of the activated coverslips or bottom plates and sandwiched with a nonactivated glass coverslip to create a flat gel. The solutions were left to polymerize for 60 min, and the nonactivated glass coverslip was peeled off, leaving the flat gel attached to the activated glass surface. The gels were allowed to swell for 1 to 3 days in 1× PBS at 37°C. After aspirating off the PBS, PA gels were coated with collagen type I as described above.

To create viscoelastic PA gels, LA was prepared by adding 0.0024% APS and 0.05% TEMED to 5% acrylamide (*30*). The solution was allowed to polymerize for 2 hours at 37°C (*30*). To generate slow and fast relaxing gels, 0.75% LA or 50% LA, respectively, was added to the aforementioned arylamide/bis-acrylamide mixtures, which were then covered from light and degassed for 20 min. Next, the gels were allowed to polymerize for 50 min on the activated glass surfaces by adding 10% APS and 0.04% TEMED.

### Lipid staining

BODIPY 493/503 (D3922, Thermo Fisher Scientific) was diluted in PBS to a final concentration of 2 μM. hMSCs were incubated with BODIPY (2 μM) for 15 min at 37°C and 5% $CO_2$. Cells were then washed twice with 1× PBS and then fixed with 4% paraformaldehyde for 15 min. Thereafter, cells were washed twice with 1× PBS and permeabilized for 15 min with 1% Triton X-100 dissolved in 1× PBS. Cells were then blocked for 1 hour with 2% BSA and 0.1% Triton X-100 and incubated for 1 hour with Hoechst (1:1000) in blocking buffer. Last, cells were washed three times with 1× PBS and imaged with a Nikon AXR confocal microscope using a Plan Apo 40×/1.15 WI (AXR) objective. Images were analyzed in ImageJ.

### Morphological analysis

hMSCs were cultured for 6 days on gels of prescribed stiffness or viscoelasticity in the presence of an adipogenic/osteogenic inducing medium of either 0.77 or 8 cP. Next, cells were fixed and stained with Hoechst (nucleus) and phalloidin (actin), as described above. Immunofluorescence images were acquired with a Nikon A1 confocal microscope using a Plan Apo 60×/1.4 NA (A1) objective or a Nikon

AXR confocal microscope using a Plan Apo 40×/1.15 WI (AXR) objective. The images were segmented to identify cellular boundaries based on the actin (568 or 647 nm) and nuclei (405 nm) channels using an open-source software called CellProfiler (*47*). This platform enabled the measurements of several shape-dependent cellular and nuclear morphological features: cell area, cell major axis length (the length of the major axis of the ellipse), cell form factor [defined as $4\pi$*(area)/perimeter$^2$], cell perimeter, cell eccentricity (defined as the ratio of the distance between the foci of an ellipse and the cell's major axis length), cell solidity (measurement of the convex region inside a cell that is calculated as object area/convex hull area), and nuclear area. Principal components analysis was also used to identify the key morphological features in the dataset that accounted for 95% of the variance for cells on elastic gels. The measured features were condensed into a 2D space using a reduced dimensionality algorithm known as the UMAP space (*48*). Unsupervised *k*-means clustering was performed to classify cells into six distinct morphological subtypes and optimal number of clusters based on silhouette scores (fig. S8). Representative *k*-means subtype morphologies were selected on the basis of geometric proximity to each cluster's center on the UMAP space.

### Membrane tension measurements

hMSCs, cultured for 6 days on 600-Pa PA gels in an adipogenic/osteogenic inducing medium of prescribed viscosity in the absence or presence of cariporide, were washed with DMEM containing 10% FBS and 1% P/S. Next, cells were stained with live-cell membrane tension probe Flipper-TR (Spirochrome, 0.5 mM) and imaged immediately thereafter. Confocal FLIM analysis of hMSCs stained with Flipper-TR was performed as previously described (*16*), using a Zeiss LSM 780 microscope and a PicoQuant system consisting of a PicoHarp 300 time-correlated single-photon counting module, two-hybrid PMA-04 detectors, and a Sepia II laser control module. The FLIM data were processed and analyzed as previously described (*16*).

### NHE1 activity measurements using $NH_4Cl$ treatment

hMSCs, cultured for 6 days on 600-Pa PA gels in the presence of an adipogenic/osteogenic inducing medium of prescribed viscosity, were washed with DMEM containing 10% FBS and 1% P/S. Next, cells were loaded with pHrodo Red AM (P35372, Thermo Fisher Scientific) dissolved in DMEM-containing medium, following the manufacturer's instructions. NHE1 activity was measured as previously described (*16*). Briefly, cells were then washed once with DMEM-containing medium and imaged in a Nikon AXR confocal microscope using a Plan Apo 40×/1.15 WI (AXR) objective every 30 s for 2 min. Cell culture medium was then gently replaced with DMEM containing 15 mM $NH_4Cl$. Cells were then imaged every 30 s for 4 min. Last, DMEM medium containing 15 mM $NH_4Cl$ was removed and replaced with 2 ml of DMEM containing 10% FBS and 1% P/S. Cells were imaged every 30 s for 5 min. A region of interest (ROI) was drawn around each cell in NIS Elements Software (Nikon) to measure pHrodo Red AM (568 nm) intensity. Data were imported into GraphPad Prism (v. 9.5.1; GraphPad, San Diego, CA) to obtain the rate of pH recovery when DMEM containing 15 mM $NH_4Cl$ was replaced with regular DMEM by using simple linear regression (*16*).

### Calcium activity measurements

hMSCs were cultured for 6 days on soft PA substrates with an adipogenic/osteogenic inducing medium of prescribed viscosity in the presence of vehicle control or inhibitors of TRPV4 (HC060747, 5 μM) or NHE1 (cariporide, 10 μM) or ILK (CPD22, 2.5 μM) or vehicle control. Cells were then washed once with 1× PBS and loaded with Fluo-4 AM (*50*) (F14201, Thermo Fisher Scientific), following the manufacturer's instructions. Thirty minutes later, cells were washed twice with 1× PBS, and fresh growth media was then added. Next, hMSCs were imaged in a Nikon AXR confocal microscope using a Plan Apo 20× (AXR) objective every minute for 20 min using the 488-nm laser. The Fluo-4 (green fluorescent protein) signal was manually traced in ImageJ overtime by drawing a circular ROI in the cell and measuring its intensity. Calcium spikes were defined as instances with intensity two times greater than the corresponding baseline levels (*16*).

### Alginate gel preparation

High molecular weight (MW) sodium alginate (average MW, 177 ± 36 kDa; LF20/40) was used to fabricate slow-relaxing alginate hydrogels. High MW alginate was irradiated by a cobalt source at a dose of 8 mrad to produce low MW (average MW, 26 ± 2 kDa) to make fast-relaxing gels (*51*). RGD-coupled alginate was prepared by coupling RGD oligopeptide (GGGGRGDSP, Peptide 2.0 Inc.) using carbodiimide chemistry, following a previously published method (*51*). Alginate was purified using dialysis membrane [3500 molecular weight cut off (MWCO), Spectra/Por 7 Dialysis Membrane] against DI $H_2O$ for 3 days, treated with activated charcoal, sterile filtered, lyophilized for 4 to 5 days, and then stored at −20°C until use. For 2% (w/v) alginate gel, the density of RGD was 1500 μM (*10*).

### Stiffness and stress relaxation measurements

Stiffness and viscoelasticity of PA gels were determined by compression testing using an E42.503 Exceed Electromechanical Test System by MTS machine. The gels, 1 to 3 mm in thickness and 8 to 25 mm in diameter, were maintained in PBS at 37°C for 24 hours before measurements. The PA gels were compressed to 15% strain with a deformation of 2 mm/min. The Young's modulus (elastic modulus) was calculated by determining the slope of the linear stress and strain curve between 5 and 10% strain. The stress relaxation corresponds to the half stress relaxation time. In select experiments, the gels were incubated for 6 days in medium of prescribed viscosities before measurements.

The initial elastic modulus and stress relaxation properties of alginate hydrogels were characterized by unconfined compression tests of disk-shaped hydrogels (15 mm in diameter and 2 mm thickness), as previously described (*10*). Before testing, hydrogels were incubated in DMEM for 24 hours. Compression was applied to the gel disks at a 15% strain with a deformation rate of 2 mm/min and a data acquisition rate of 100 Hz using an MTS Criterion Series 40 Tensile Tester. The initial elastic modulus was calculated on the basis of the slope of the stress-strain curve (5 to 10% strain linear part). For the stress relaxation properties, after being compressed to 15% strain, the compression strain was kept at 15%, and the load was recorded over time. The relaxation $t_{1/2}$ was measured as the time for the stress decreased to half of its maximum value.

### 2D cell culture on alginate gels

One- and 2-mm-thick alginate hydrogels were prepared for slow-relaxing and fast-relaxing gels, respectively. Briefly, RGD-coupled alginates with different MW were reconstituted in DMEM to 2.5% (w/v) and rapidly mixed with DMEM containing the appropriate

amount of calcium sulfate ($CaSO_4$) to form alginate hydrogels with a final concentration of 2% (w/v) and a stiffness of 20 kPa. High and low MW sodium alginates were mixed with $CaSO_4$ at final $Ca^{2+}$ concentrations of 23 and 65 mM, respectively. After gelling for 45 min, gels were punched into 15-mm-diameter gel disks and were equilibrated in DMEM overnight. For the 2D cell culture, gel disks were held at the bottom of well plates by a plastic transwell holder without the membrane. hMSCs were seeded at a density of 7000 cells/$cm^2$ inside the holder.

### Von Kossa staining

After 6 days of culture in an adipogenic/osteogenic inducing medium of prescribed viscosity, hMSCs were washed three times with 1× PBS and fixed with paraformaldehyde for 15 min. Cells were then stained with the Von Kossa kit (1.00362, Sigma-Aldrich) by adding 300 μl of reagent 1 and exposing them to UV light for 30 min. Next, cells were washed twice with DI $H_2O$, and 300 μl of reagent 2 was added for 20 min. Last, cells were washed with DI $H_2O$ twice and imaged using a Nikon A1 confocal microscope using a Plan Apo 10×/1.4 NA objective.

### ALP staining

After 6 days of culture in an adipogenic/osteogenic inducing medium of prescribed viscosity, hMSCs were washed three times with 1× PBS and fixed with paraformaldehyde for 1 min. Cells were then stained with the Alkaline Phosphatase Detection Kit (SCR004, Sigma-Aldrich) following the manufacturer's instructions. Cells were imaged using a Nikon Ti2 bright-field microscope with a Plan Apo 10×/1.4 NA objective.

### Macrophage differentiation

hMSCs were cultured for 3 days on PA gels of prescribed stiffness at specified (0.77 or 8 cP) extracellular fluid viscosities. Thereafter, the hMSC medium was aspirated off and replaced with medium of the same viscosity containing interferon-γ (IFN-γ; 2.5 ng/μl; 570204, BioLegend). One day later, the IFN-γ–containing medium was replaced with macrophage culture medium consisting of RPMI 1640 (11875093, Gibco) supplemented with 10% FBS, 1% P/S, 10 mM Hepes (15630080, Thermo Fisher Scientific), 50 pM β-mercaptoethanol (21985023, Thermo Fisher Scientific), 1 mM sodium pyruvate (11360070, Thermo Fisher Scientific), and 200 mM glutamine (25030149, Thermo Fisher Scientific). After 2 days of incubation, this medium was collected and used to treat M0 macrophages. M0 macrophages were generated from THP1 cells that had been pretreated for 2 days with phorbol 12-myristate 13-acetate (200 nM; P1585-1MG, Sigma-Aldrich) in RPMI-containing complete medium. Macrophages were next incubated for 2 days with the RPMI-conditioned medium collected from hMSCs, and their differentiation was evaluated via qPCR, immunofluorescence, or Western blotting.

### Proteome profiler array

hMSCs were cultured for 3 days on 600-Pa PA gels at specified (0.77 or 8 cP) extracellular fluid viscosities. Thereafter, the hMSC medium was aspirated off and replaced with medium of the same viscosity containing IFN-γ (2.5 ng/μl). One day later, the IFN-γ–containing medium was replaced with macrophage culture medium consisting of RPMI 1640 supplemented with 10% FBS, 1% P/S, 10 mM Hepes, 50 pM β-mercaptoethanol, 1 mM sodium pyruvate, and 200 mM glutamine. The RPMI-conditioned medium was then collected and tested for cytokine secretion using the Proteome Profiler Human Cytokine Array Kit (ARY005B, R&D Systems) following the manufacturer's instructions. The resulting array was developed using 20% SuperSignal West Atto (A38555, Thermo Fisher Scientific) diluted in DI $H_2O$.

### Western blotting

Western blots were performed as previously described (*23*). hMSCs, cultured for 6 days on 600-Pa PA gels with an adipogenic/osteogenic inducing medium of either 0.77 or 8 cP, were washed three times with 1 ml of 1× PBS, and 2 ml of 0.05% trypsin (25300120, Thermo Fisher Scientific) was then added to the cells. Once the cells were detached, 7 ml of growth media was added to the gels, and cells were collected and centrifuged for 5 min at 0.3*g*. The cell pellet was then resuspended in 1 ml of 1× PBS and centrifuged for 5 min at 0.3*g*. Next, the cell pellet was lysed with 60 μl of radioimmunoprecipitation assay (RIPA) buffer (R0278, Sigma-Aldrich) containing protease/phosphatase inhibitor (1:100; 5872S, Cell Signaling) and collected into 1.5-ml Eppendorf tubes. After vortexing for 1 min, cell lysates were left on ice for 1 hour and then centrifuged for 10 min at 14,000*g*. Protein concentrations were quantified using the Pierce BCA Protein Assay (Thermo Fisher Scientific) to ensure equal protein loading across all conditions. Specimens were boiled for 10 min at 97°C, then left on ice for 1 min, and centrifuged at 14,000*g* for 1 min. Samples were loaded into a 4 to 12% bis-tris gel (NP0336BOX, Invitrogen) as previously described (*49*), and the gel was run at 200 V for ~50 min. Proteins were transferred from the gel onto a polyvinylidene difluoride membrane (1704272, Bio-Rad) at 1.3 mA/25 V for 7 to 10 min at room temperature and blocked with 5% nonfat milk for 1 hour followed by overnight incubation at 4°C with primary antibodies: anti-NHE1 (1:200; sc-136239, Santa Cruz Biotechnology), glyceraldehyde phosphate dehydrogenase (14C10) (1:4000; 2118, Cell Signaling), and anti-ILK (1:200; sc-20019, Santa Cruz Biotechnology). Next, membranes were washed five times with 1× Tris-buffered saline with Tween 20 (TBST) for 5 min and incubated for 1 hour at room temperature with anti-mouse immunoglobulin G (IgG) horseradish peroxidase (HRP)–linked antibody (1:2000; 7076, Cell Signaling) or anti-rabbit IgG HRP-linked antibody (1:2000; 7074, Cell Signaling). After washing five times with 1× TBST for 5 min, membranes were developed and imaged. The resulting images were quantified with ImageJ.

Western blotting of THP1-derived macrophages was also performed as described above, albeit with the following modifications. Macrophages were washed twice with 1 ml of ice-cold 1× PBS, lysed with 80 μl of RIPA buffer containing protease/phosphatase inhibitor, and collected using a cell scraper into 1.5-ml Eppendorf tubes. Anti-Arginase 1 (1:50; sc-166920, Santa Cruz Biotechnology) was used as the primary antibody and α-tubulin (1:1000; sc-5286, Santa Cruz Biotechnology) as the loading control.

### Statistical analysis and reproducibility

Data are the mean ± SD of three or more experiments (reflecting independent biological replicas) unless otherwise indicated. Data points represent values from each cell or experiment as detailed in the figure legends. The Shapiro-Wilk test was used to test normality when the number of data points was between 3 and 8. For experiments with >8 data points, the D'Agostino-Pearson omnibus normality test was used to assess whether data were normally distributed. Datasets with normal distributions were evaluated using the Student's

*t* test (two-tailed) or one-way analysis of variance (ANOVA) followed by Tukey's or Dunnett's post hoc test. For log normal distributions, comparisons were made after logarithmic transformation of the data followed by appropriate statistical test (unpaired Student's *t* test or one-way ANOVA). For non-Gaussian distributions, the nonparametric Mann-Whitney test or Kruskal-Wallis test followed by Dunn's multiple comparisons was used where appropriate. Analysis was performed using GraphPad Prism 10 (GraphPad Software). Statistical significance was identified as $P < 0.05$. $^{*}P < 0.05$, $^{**}P < 0.01$, $^{***}P < 0.001$, and $^{****}P < 0.0001$.

## Supplementary Materials

**This PDF file includes:**

Figs. S1 to S8

## REFERENCES AND NOTES


1. J. Zhou, Y. Shi, Mesenchymal stem/stromal cells (MSCs): Origin, immune regulation, and clinical applications. *Cell. Mol. Immunol.* **20**, 555–557 (2023).
2. B. M. Abdallah, M. Kassem, Human mesenchymal stem cells: From basic biology to clinical applications. *Gene Ther.* **15**, 109–116 (2008).
3. A. Abbasi, S. Imaichi, V. Ling, A. Shukla, Mesenchymal stem cell behavior on soft hydrogels with aligned surface topographies. *ACS Appl. Bio. Mater.* **5**, 1890–1900 (2022).
4. W. Zhai, J. Tan, T. Russell, S. Chen, D. McGonagle, M. Win Naing, D. Yong, E. Jones, Multi-pronged approach to human mesenchymal stromal cells senescence quantification with a focus on label-free methods. *Sci. Rep.* **11**, 1054 (2021).
5. C. Yang, M. W. Tibbitt, L. Basta, K. S. Anseth, Mechanical memory and dosing influence stem cell fate. *Nat. Mater.* **13**, 645–652 (2014).
6. N. Huebsch, P. R. Arany, A. S. Mao, D. Shvartsman, O. A. Ali, S. A. Bencherif, J. Rivera-Feliciano, D. J. Mooney, Harnessing traction-mediated manipulation of the cell/matrix interface to control stem-cell fate. *Nat. Mater.* **9**, 518–526 (2010).
7. A. J. Engler, S. Sen, H. L. Sweeney, D. E. Discher, Matrix elasticity directs stem cell lineage specification. *Cell* **126**, 677–689 (2006).
8. M. Geerligs, G. W. M. Peters, P. A. J. Ackermans, C. W. J. Oomens, F. P. T. Baaijens, Linear viscoelastic behavior of subcutaneous adipose tissue. *Biorheology* **45**, 677–688 (2008).
9. Z. Liu, L. Bilston, On the viscoelastic character of liver tissue: Experiments and modelling of the linear behaviour. *Biorheology* **37**, 191–201 (2000).
10. O. Chaudhuri, L. Gu, D. Klumpers, M. Darnell, S. A. Bencherif, J. C. Weaver, N. Huebsch, H.-P. Lee, E. Lippens, G. N. Duda, D. J. Mooney, Hydrogels with tunable stress relaxation regulate stem cell fate and activity. *Nat. Mater.* **15**, 326–334 (2016).
11. R. E. Wells Jr., E. W. Merrill, Shear rate dependence of the viscosity of whole blood and plasma. *Science* **133**, 763–764 (1961).
12. J. Gonzalez-Molina, X. Zhang, M. Borghesan, J. Mendonca da Silva, M. Awan, B. Fuller, N. Gavara, C. Selden, Extracellular fluid viscosity enhances liver cancer cell mechanosensing and migration. *Biomaterials* **177**, 113–124 (2018).
13. R. J. Ellis, Macromolecular crowding: Obvious but underappreciated. *Trends. Biochem. Sci.* **26**, 597–604 (2001).
14. P. W. Rand, E. Lacombe, H. E. Hunt, W. H. Austin, Viscosity of normal human blood under normothermic and hypothermic conditions. *J. Appl. Physiol.* **19**, 117–122 (1964).
15. S. Sarkar, T. S. Rosenkrantz, Neonatal polycythemia and hyperviscosity. *Semin. Fetal Neonatal Med.* **13**, 248–255 (2008).
16. K. Bera, A. Kiepas, I. Godet, Y. Li, P. Mehta, B. Ifemembi, C. D. Paul, A. Sen, S. A. Serra, K. Stoletov, J. Tao, G. Shatkin, S. J. Lee, Y. Zhang, A. Boen, P. Mistriotis, D. M. Gilkes, J. D. Lewis, C.-M. Fan, A. P. Feinberg, M. A. Valverde, S. X. Sun, K. Konstantopoulos, Extracellular fluid viscosity enhances cell migration and cancer dissemination. *Nature* **611**, 365–373 (2022).
17. K. Lee, Y. Chen, T. Yoshitomi, N. Kawazoe, Y. Yang, G. Chen, Osteogenic and adipogenic differentiation of mesenchymal stem cells in gelatin solutions of different viscosities. *Adv. Healthc. Mater.* **9**, e2000617 (2020).
18. J. Zheng, Y. Wang, N. Kawazoe, Y. Yang, G. Chen, Influences of viscosity on the osteogenic and adipogenic differentiation of mesenchymal stem cells with controlled morphology. *J. Mater. Chem. B* **10**, 3989–4001 (2022).
19. Y.-Q. Chen, M.-C. Wu, M.-T. Wei, J.-C. Kuo, H. W. Yu, A. Chiou, High-viscosity driven modulation of biomechanical properties of human mesenchymal stem cells promotes osteogenic lineage. *Mater. Today Bio* **26**, 101058 (2024).
20. A. Afthinos, K. Bera, J. Chen, A. Ozcelikkale, A. Amitrano, M. I. Choudhury, R. Huang, P. Pachidis, P. Mistriotis, Y. Chen, K. Konstantopoulos, Migration and 3D traction force measurements inside compliant microchannels. *Nano Lett.* **22**, 7318–7327 (2022).
21. S. Dupont, L. Morsut, M. Aragona, E. Enzo, S. Giulitti, M. Cordenonsi, F. Zanconato, J. Le Digabel, M. Forcato, S. Bicciato, N. Elvassore, S. Piccolo, Role of YAP/TAZ in mechanotransduction. *Nature* **474**, 179–183 (2011).
22. S. M. Engels, P. Kamat, G. S. Pafilis, Y. Li, A. Agrawal, D. J. Haller, J. M. Phillip, L. M. Contreras, Particulate matter composition drives differential molecular and morphological responses in lung epithelial cells. *PNAS Nexus* **3**, pgad415 (2024).
23. Y. Zhang, Y. Li, K. N. Thompson, K. Stoletov, Q. Yuan, K. Bera, S. J. Lee, R. Zhao, A. Kiepas, Y. Wang, P. Mistriotis, S. A. Serra, J. D. Lewis, M. A. Valverde, S. S. Martin, S. X. Sun, K. Konstantopoulos, Polarized NHE1 and SWELL1 regulate migration direction, efficiency and metastasis. *Nat. Commun.* **13**, 6128 (2022).
24. C. Wu, S. Dedhar, Integrin-linked kinase (ILK) and its interactors: A new paradigm for the coupling of extracellular matrix to actin cytoskeleton and signaling complexes. *J Cell Biol* **155**, 505–510 (2001).
25. C. Ji, M. Zhang, J. Hu, C. Cao, Q. Gu, Y. Liu, X. Li, D. Xu, L. Ying, Y. Yang, H. Gao, J. Li, L. Yu, The kinase activity of integrin-linked kinase regulates cellular senescence in gastric cancer. *Cell Death Dis.* **13**, 577 (2022).
26. Y. Li, K. Konstantopoulos, R. Zhao, Y. Mori, S. X. Sun, The importance of water and hydraulic pressure in cell dynamics. *J Cell Sci* **133**, jcs240341 (2020).
27. J. S. Silver, K. A. Gunay, A. A. Cutler, T. O. Vogler, T. E. Brown, B. T. Pawlikowski, O. J. Bednarski, K. L. Bannister, C. J. Rogowski, A. G. McKay, F. W. DelRio, B. B. Olwin, K. S. Anseth, Injury-mediated stiffening persistently activates muscle stem cells through YAP and TAZ mechanotransduction. *Sci. Adv.* **7**, eabe4501 (2021).
28. A. Kaneda, T. Seike, T. Danjo, T. Nakajima, N. Otsubo, D. Yamaguchi, Y. Tsuji, K. Hamaguchi, M. Yasunaga, Y. Nishiya, M. Suzuki, J.-I. Saito, R. Yatsunami, S. Nakamura, Y. Sekido, K. Mori, The novel potent TEAD inhibitor, K-975, inhibits YAP1/TAZ-TEAD protein-protein interactions and exerts an anti-tumor effect on malignant pleural mesothelioma. *Am. J. Cancer Res.* **10**, 4399–4415 (2020).
29. O. Chaudhuri, J. Cooper-White, P. A. Janmey, D. J. Mooney, V. B. Shenoy, Effects of extracellular matrix viscoelasticity on cellular behaviour. *Nature* **584**, 535–546 (2020).
30. E. E. Charrier, K. Pogoda, R. Li, C. Y. Park, J. J. Fredberg, P. A. Janmey, A novel method to make viscoelastic polyacrylamide gels for cell culture and traction force microscopy. *APL Bioeng.* **4**, 036104 (2020).
31. O. Chaudhuri, L. Gu, M. Darnell, D. Klumpers, S. A. Bencherif, J. C. Weaver, N. Huebsch, D. J. Mooney, Substrate stress relaxation regulates cell spreading. *Nat. Commun.* **6**, 6364 (2015).
32. A. Bauer, L. Gu, B. Kwee, W. A. Li, M. Dellacherie, A. D. Celiz, D. J. Mooney, Hydrogel substrate stress-relaxation regulates the spreading and proliferation of mouse myoblasts. *Acta Biomater.* **62**, 82–90 (2017).
33. A. Y. Clark, K. E. Martin, J. R. Garcia, C. T. Johnson, H. S. Theriault, W. M. Han, D. W. Zhou, E. A. Botchwey, A. J. Garcia, Integrin-specific hydrogels modulate transplanted human bone marrow-derived mesenchymal stem cell survival, engraftment, and reparative activities. *Nat. Commun.* **11**, 114 (2020).
34. M. Francois, R. Romieu-Mourez, M. Li, J. Galipeau, Human MSC suppression correlates with cytokine induction of indoleamine 2,3-dioxygenase and bystander M2 macrophage differentiation. *Mol. Ther.* **20**, 187–195 (2012).
35. Z. Liu, J. Liu, J. Li, Y. Li, J. Sun, Y. Deng, H. Zhou, Substrate stiffness can affect the crosstalk between adipose derived mesenchymal stem cells and macrophages in bone tissue engineering. *Front. Bioeng. Biotechnol.* **11**, 1133547 (2023).
36. A. S. Caldwell, V. V. Rao, A. C. Golden, D. J. Bell, J. C. Grim, K. S. Anseth, Mesenchymal stem cell-inspired microgel scaffolds to control macrophage polarization. *Bioeng. Transl. Med.* **6**, e10217 (2021).
37. M. Darnell, L. Gu, D. Mooney, RNA-seq reveals diverse effects of substrate stiffness on mesenchymal stem cells. *Biomaterials* **181**, 182–188 (2018).
38. A. Vilar, M. Hodgson-Garms, G. D. Kusuma, I. Donderwinkel, J. Carthew, J. L. Tan, R. Lim, J. E. Frith, Substrate mechanical properties bias MSC paracrine activity and therapeutic potential. *Acta Biomater.* **168**, 144–158 (2023).
39. Y. Song, Y. Zhang, Z. Wang, Y. Lin, X. Cao, X. Han, G. Li, A. Hou, S. Han, CCL2 mediated IKZF1 expression promotes M2 polarization of glioma-associated macrophages through CD84-SHP2 pathway. *Oncogene* **43**, 2737–2749 (2024).
40. K. Mortezaee, J. Majidpoor, Roles for macrophage-polarizing interleukins in cancer immunity and immunotherapy. *Cell. Oncol.* **45**, 333–353 (2022).
41. C. Peng, G. Tu, J. Wang, Y. Wang, P. Wu, L. Yu, Z. Li, X. Yu, MLKL signaling regulates macrophage polarization in acute pancreatitis through CXCL10. *Cell Death Dis.* **14**, 155 (2023).
42. Y. Ye, L. Li, H. Kang, Z. Wan, M. Zhang, B. Gang, J. Liu, G. Liu, W. Gu, LAMP1 controls CXCL10-CXCR3 axis mediated inflammatory regulation of macrophage polarization during inflammatory stimulation. *Int. Immunopharmacol.* **132**, 111929 (2024).
43. C. Moratal, J. Raffort, N. Arrighi, S. Rekima, S. Schaub, C. A. Dechesne, G. Chinetti, C. Dani, IL-1β- and IL-4-polarized macrophages have opposite effects on adipogenesis of intramuscular fibro-adipogenic progenitors in humans. *Sci. Rep.* **8**, 17005 (2018).

44. F. Nie, J. Zhang, H. Tian, J. Zhao, P. Gong, H. Wang, S. Wang, P. Yang, C. Yang, The role of CXCL2-mediated crosstalk between tumor cells and macrophages in *Fusobacterium nucleatum*-promoted oral squamous cell carcinoma progression. *Cell Death Dis.* **15**, 277 (2024).
45. Z. Bian, X. Wu, Q. Chen, Q. Gao, X. Xue, Y. Wang, Oct4 activates IL-17A to orchestrate M2 macrophage polarization and cervical cancer metastasis. *Cancer Immunol. Immunother.* **73**, 73 (2024).
46. B. A. Castro, P. Flanigan, A. Jahangiri, D. Hoffman, W. Chen, R. Kuang, M. De Lay, G. Yagnik, J. R. Wagner, S. Mascharak, M. Sidorov, S. Shrivastav, G. Kohanbash, H. Okada, M. K. Aghi, Macrophage migration inhibitory factor downregulation: A novel mechanism of resistance to anti-angiogenic therapy. *Oncogene* **36**, 3749–3759 (2017).
47. D. R. Stirling, M. J. Swain-Bowden, A. M. Lucas, A. E. Carpenter, B. A. Cimini, A. Goodman, CellProfiler 4: Improvements in speed, utility and usability. *BMC Bioinformatics* **22**, 433 (2021).
48. E. Becht, L. McInnes, J. Healy, C.-A. Dutertre, I. W. H. Kwok, L. G. Ng, F. Ginhoux, E. W. Newell, Dimensionality reduction for visualizing single-cell data using UMAP. *Nat. Biotechnol.* **37**, 38–48 (2018).
49. R. A. Law, A. Kiepas, H. E. Desta, E. Perez Ipina, M. Parlani, S. J. Lee, C. L. Yankaskas, R. Zhao, P. Mistriotis, N. Wang, Z. Gu, P. Kalab, P. Friedl, B. A. Camley, K. Kon stantopoulos, Cytokinesis machinery promotes cell dissociation from collectively migrating strands in confinement. *Sci. Adv.* **9**, eabq6480 (2023)
50. R. Zhao, A. Afthinos, T. Zhu, P. Mistriotis, Y. Li, S. A. Serra, Y. Zhang, C. L. Yankaskas, S. He, M. A. Valverde, S. X. Sun, K. Konstantopoulos, Cell sensing and decision-making in confinement: The role of TRPM7 in a tug of war between hydraulic pressure and cross-sectional area. *Sci. Adv.* **5**, eaaw7243 (2019).
51. J. A. Rowley, G. Madlambayan, D. J. Mooney, Alginate hydrogels as synthetic extracellular matrix materials. *Biomaterials* **20**, 45–53 (1999).


**Acknowledgments:** We wish to thank C. Min for developing the algorithm and software used in cell morphological analysis. **Funding:** This work was supported, in part, by R01 CA 257647 (K.K.), R01 GM142175 (K.K. and L.G.), Maryland Stem Cell Research Fund [2025-MSCRFL-0025 (K.K. and L.G.) and 2024-MSCRFL-6272 (L.G.)], R56 HL169764 (L.G.), T32 AG058527 (Y.W.D.), P30 AG021334 (J.M.P.), and AFAR Junior Faculty Award (J.M.P.). The opinions, findings, and conclusions, or recommendations expressed are those of the authors and do not necessarily reflect the views of any of the funding agencies. **Author contributions:** Conceptualization: A.A., Q.Y., B.A., A.S., Y.Z., L.G., and K.K. Investigation: A.A., Q.Y., B.A., A.S., Y.W.D., and Y.Z. Visualization: A.A., Q.Y., B.A., A.S., Y.Z., Y.W.D., and K.K. Writing—original draft: A.A., Q.Y., and K.K. Writing—review and editing: A.A., Q.Y., B.A., A.S., J.M.P., L.G., and K.K. Methodology: A.A., Q.Y., B.A., A.S., Y.W.D., Y.Z., J.M.P., L.G., and K.K. Data curation: A.A., Q.Y., Y.W.D., and K.K. Validation: A.A., Q.Y., B.A., A.S., Y.W.D., Y.Z., J.M.P., L.G., and K.K. Formal analysis: A.A., Q.Y., B.A., Y.Z., and Y.W.D. Software: Y.W.D. and J.M.P. Funding acquisition: J.M.P., L.G., and K.K. Resources: L.G., J.M.P., and K.K. Supervision: J.M.P., L.G., and K.K. Project administration: K.K. **Competing interests:** The authors declare that they have no competing interests. **Data and materials availability:** All data needed to evaluate the conclusions in the paper are present in the paper and/or the Supplementary Materials. All source data are provided with this paper.

Submitted 3 July 2024
Accepted 20 November 2024
Published 1 January 2025
10.1126/sciadv.adr5023